Information entropies with Varshni-Hellmann potential in higher dimensions

Etido P. Inyang[a,b*], A.E.L. Aouami[d] , N. Ali[b,c], R. Endut[b,c], N.R. Ali[f] , S.A. Aljunid[b,c]

A Department of Physics, National Open University of Nigeria, Jabi-Abuja, Nigeria
B Faculty of Electronic Engineering & Technology, Universiti Malaysia Perlis, 02600 Arau, Perlis, Malaysia
C Centre of Excellence Advanced Communication Engineering (ACE), Universiti Malaysia Perlis, 02600 Arau, Perlis, Malaysia
D Group of Optoelectronic of Semiconductors and Nanomaterials, ENSAM, Mohammed V University in Rabat, Rabat, 10100, Morocco
F School of Electrical and Electronic Engineering, Universiti Sains Malaysia, Engineering Campus, Nibong Tebal, Penang, Malaysia.

E-mail: einyang@noun.edu.ng

Abstract

This work investigates the behavior of Shannon entropy and Fisher information for the Varshni-Hellmann potential (VHP) in one and three dimensions using the Nikiforov-Uvarov method. We employ the Greene-Aldrich approximation scheme to obtain the energy eigenvalues and normalized wavefunctions, which are then used to calculate these information-theoretic quantities. Our analysis revealed remarkably similar high-order features in both position and momentum spaces. Notably, our calculations showed enhanced accuracy in predicting particle localization within position space. Furthermore, the combined position and momentum entropies obeyed the lower and upper bounds established by the Berkner-Bialynicki-Birula-Mycieslki inequality. Additionally, for three-dimensional systems, the Stam-Cramer-Rao inequalities were fulfilled for different eigenstates with respect to the calculated Fisher information. It is observed that as the position Fisher entropy decreases, indicating a more precise measurement of position, the momentum Fisher entropy must increase. This implies that the Fisher information regarding momentum decreases, resulting in a decrease in the precision of momentum measurement. This demonstrates how position and momentum uncertainties complement each other in quantum mechanics. Exploring the balance between position and momentum Fisher entropy reveals a fundamental aspect of the uncertainty principle in quantum mechanics, highlighting the restrictions on measuring certain pairs of conjugate variables simultaneously with high precision.

Keywords: Schrodinger equation; Stam-Cramer-Rao inequality, Nikiforov-Uvarov method; Shannon entropy; Fisher information.

1. Introduction

In non-relativistic quantum mechanics, both exact and approximate solutions of the Schrodinger equation (SE) hold significant value due to their unique properties. This is as a result of the useful information that the wave functions and eigenvalues provide in describing various quantum systems like atomic structure theory, information theory, quantum electrodynamics, quantum dots, and more [1-5]. Exploring the fundamental principles that govern the processing and transmission of information in quantum systems is a key focus of quantum information theory, a branch of quantum mechanics and information theory. Various researchers have made significant efforts to address the SE through diverse analytical approaches [6–10] to handle the superposition of various potentials, enabling a broader spectrum of applications [11]. For instance, Inyang et al. [12] examined the mass spectra of heavy mesons using the combination of the Hulthern and Hellmann potential models. Quantum information theory heavily relies on two key concepts: global Shannon entropy and Fisher information (FI) [13]. These concepts, rooted in Claude Shannon's information theory principles [14], have found applications in communication theory, as evidenced by their use in various studies [15-17]. While Fisher information's theoretical foundation was established earlier [18], its practical significance remained elusive until Sear et al. [19] demonstrated its connection to the kinetic energy of quantum systems. Besides Shannon and FI, other global measures include Tsallis, Renyi, and Onicescu energy [20–22]. Understanding the uncertainty associated with a probability distribution is crucial, as highlighted in previous studies [23-26]. Berkner, Bialynicki-Birula, and Mycieslki (BBM) [27] explored this concept by establishing an entropic connection between the position and momentum spaces (PMS) using

Shannon entropy, denoted by $S(\rho_{nl})+S(\gamma_{nl})\geq D(1+\ln\pi)$, where D represents the number of spatial dimensions. This relationship has been demonstrated to be more advanced than the Heisenberg uncertainty relation (HUR), as it can accommodate a higher level of complexity. The Shannon entropy expression is defined as follows:

$$S(\rho_{nl})=-\int_{R^D}\rho_{nl}(r_q)\ln\rho_{nl}(r_q)dr_q \tag{1}$$

and

$$S(\gamma_{nl})=-\int_{R^D}\gamma_{nl}(p)\ln\gamma_{nl}(p)dp \tag{2}$$

where $S(\rho_{nl})$ is the position space Shannon entropy, $S(\gamma_{nl})$ is the momentum space Shannon entropy,

and the probability densities (PD) in the position and momentum spaces, are given in Eq.(3) and (4) respectively.

$$\rho(r_q)=\left|\psi(r_q)\right|^2 \tag{3}$$

and

$$\rho(p)=\left|\psi(p)\right|^2 \tag{4}$$

$\psi(p)$ represents the momentum-space wave function, which is the result of applying the Fourier transform (FT) of $\psi(r_q)$. Shannon entropy quantifies the level of unpredictability and disorder within a specific area. In quantum mechanics, the spread of a particle's momentum is captured by momentum entropy, derived from the position space through a Fourier transform. This concept is linked to Shannon entropy and reflects the degree of localization or delocalization of a system [28-30]. Conversely, FI, as the only part of the local measure, focuses mainly on local alterations in PD. The FI, is expressed as follows [23, 24]:

$$I(\rho)=\int_{R^D}\frac{\left|\nabla\rho_{nl}(r_q)\right|^2}{\rho_{nl}(r_q)}dr_q \tag{5}$$

$$I(\gamma)=\int_{R^D}\frac{\left|\nabla\rho_{nl}(p)\right|^2}{\rho_{nl}(p)}dp \tag{6}$$

Fisher information inequality becomes [23]

$$I(\rho)I(\gamma)\geq 9\left[2-\frac{2l+1}{l(l+1)}|m|\right]^2\geq 36 \tag{7}$$

The uncertainty relation utilized to validate the FI measure for any central potential is known as the Stam-Cramer-Rao (SCR) inequality [33]. Onyeaju et al. [34] derived the wave equation utilizing a molecular potential function. The wave function was utilized to analyze information-theoretic measures (ITM) like Shannon and Renyi entropic densities. The expectation value in position and momentum spaces was calculated to confirm the HUR. Laguna et al. [35] investigated the ITM using Gaussian-type functions. Njoku et al. [36] utilized the Mobius squared plus Eckart (MMSE) potential to study the ITM and complexity. The study confirmed that the BBM inequality, the lower bound of complexity, and the FI sum inequality, were all validated for the system. Furthermore, Ayedun and colleagues [37] explored the FI and Shannon entropy using the Eckart-Hellmann potential, and their findings meet the lower-bound BBM and SCR inequalities. Similarly, Estañon et al. [38] used informational measures to study helium atoms in impenetrable spherical cavities. The cavity radius-based energies and wave functions of the confined helium atom were calculated using the Ritz variational method. Various ITMs, including Shannon entropy, FI, and Kullback-Leibler entropy, were calculated and revealed to be responsive to electronic correlation. Njoku et al. [39] calculated the energy and wave function to analyze the Shannon information entropy of the system. The BBM was authenticated for the system. Several authors have studied quantum information related to harmonic oscillators in one, two, and three dimensions [40, 41]. We aim to extensively explore combined exponential-type potential models in our current paper. The Varshni and Hellmann potential (VHP) model has not been explored for quantum information theoretic measures, as far as we know. We aim to further explore the research conducted by Inyang et al. [42] by focusing on information theoretic measures such as Shannon entropy and Fisher information in one and three dimensions. To achieve this, we will employ the Nikiforov Uvarov (NU) method for solving the SE.

The VHP is of the form:

$$V(r_q)=a-\frac{abe^{-\alpha r_q}}{r_q}-\frac{c}{r_q}+\frac{de^{-\alpha r_q}}{r_q} \tag{8}$$

where a , b, c and d are the strengths of the VHP, r_q is the inter-nuclear distance, and α is the screening parameter that dictates the form of the potential energy curve depicted in Figure 1. In atomic and plasma physics, researchers have employed the Hellmann potential [43] to investigate various phenomena [44-47]. The Varshni potential [48] is a short-range repulsive potential energy function. It is essential in chemical and molecular physics. This potential has been explored by several authors, as referenced in [49, 50]. The paper is structured as outlined below. In Section 2, we present the energy eigenvalues and the normalized wave functions. Section 3 focuses on analyzing our findings. Section 4 provides a concise conclusion.

2. Solutions for bound states of the Schrödinger equation involving Varshni and Hellmann potentials

The SE is represented by [51].

$$\frac{d^2R_{nl}(r_q)}{dr_q^{\,2}}+\left[\frac{2m}{\hbar^2}\left(E_{nl}-V(r_q)\right)-\frac{l(l+1)}{r_q^{\,2}}\right]R_{nl}(r_q)=0 \tag{9}$$

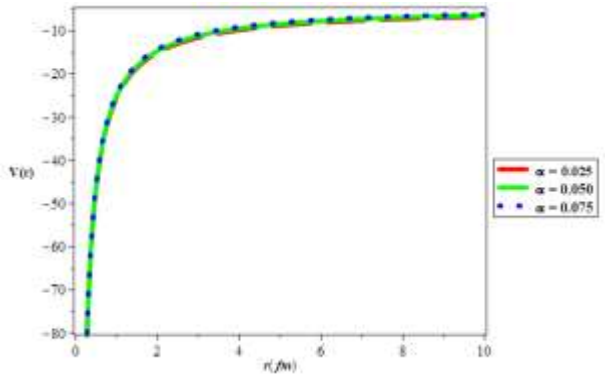

Fig. 1: Variation of the combined potential as a function of r for various values of α .

where m is the reduced mass, E_{nl} is the energy spectrum, $\hbar$ is the reduced Planck's constant, respectively. Equation (9) is solved analytically using the Greene-Aldrich approximation scheme [52] to address the centrifugal barrier. This approximation scheme is a reliable method for approximating the centrifugal barrier and is valid for a certain range of values ($\alpha \ll 1$). The scheme is expressed as:

$$\frac{1}{r_q^{\,2}} \approx \frac{\alpha^2}{\left(1-e^{-\alpha r_q}\right)^2} \tag{10}$$

Substituting Eq. (8) and Eq. (10) into Eq. (9) and using coordinate transformation $x_c = e^{-\alpha r_q}$ we have

$$\frac{d^2R(x_c)}{dx_c^{\,2}} + \frac{1-x_c}{x_c\left(1-x_c\right)}\frac{dR(x_c)}{dx_c} + \frac{1}{x_c^{\,2}\left(1-x_c\right)^2}\left[\begin{matrix}-\left(\varepsilon+\beta_a\right)x_c^{\,2}+\left(2\varepsilon+\beta_a-\beta_b\right)x_c \\ -\left(\varepsilon-\beta_b+\gamma\right)\end{matrix}\right]R(x_c)=0 \tag{11}$$

where

$$-\varepsilon = \frac{2mE_{nl}}{\hbar^2\alpha^2} - \frac{2am}{\hbar^2\alpha^2}, \quad \beta_a = \frac{2abm}{\hbar^2\alpha} - \frac{2dm}{\hbar^2\alpha}, \quad \beta_b = \frac{2cm}{\hbar^2\alpha}, \quad \gamma = l\left(l+1\right) \tag{12}$$

Comparing Eqs. (11) and (A1) ,we have the following parameters

$$\left.\begin{matrix}\sigma(x_c) = \\ -\left(\varepsilon+\beta_a\right)x_c^{\,2}+\left(2\varepsilon+\beta_a-\beta_b\right)x_c-\left(\varepsilon-\beta_b+\gamma\right), \\ \sigma(x_c)=x_c\left(1-x_c\right),\ \tilde{\tau}(x_c)=1-x_c\end{matrix}\right\} \tag{13}$$

Substituting Eq. (13) into Eq. (A9), we obtain

$$\pi(x_c) = -\frac{x_c}{2} \pm \sqrt{\left(A_a-k_a\right)x_c^{\,2}+\left(k_a+B_a\right)x_c+C_a} \tag{14}$$

where

$$\left.\begin{matrix}A_a = \frac{1}{4}+\varepsilon+\beta_a,\ B_a = \\ -\left(2\varepsilon+\beta_a-\beta_b\right),\ C_a = \varepsilon-\beta_b+\gamma\end{matrix}\right\} \tag{15}$$

To determine the constant k_a, the discriminant of the expression within the square root in Equation (14) must be set to zero. Therefore, we have

$$k_a = \beta_a+\beta_b-2\gamma \pm 2\sqrt{\varepsilon-\beta_b+\gamma}\sqrt{\gamma+\frac{1}{4}} \tag{16}$$

By substituting Equation (16) into Equation (14), we get

$$\pi(x_c) = -\frac{x_c}{2} \pm \left(\sqrt{\varepsilon-\beta_b+\gamma}+\sqrt{\gamma+\frac{1}{4}}\right)x_c - \sqrt{\varepsilon-\beta_b+\gamma} \tag{17}$$

Calculating $\tau(x_c)$ as

$$\tau\left(x_c\right) = 1-2x_c-2\sqrt{\varepsilon-\beta_b+\gamma}x_c - 2\sqrt{\gamma+\frac{1}{4}}x_c + 2\sqrt{\varepsilon-\beta_b+\gamma} \tag{18}$$

Equation (18) yields Equation (19) as

$$\tau'(x_c) = -2-2\left(\sqrt{\varepsilon-\beta_b+\gamma}+\sqrt{\gamma+\frac{1}{4}}\right) \tag{19}$$

According to Equation (A10), we define the constant λ as

$$\lambda = -\frac{1}{2} - \sqrt{\varepsilon-\beta_b+\gamma} - \sqrt{\gamma+\frac{1}{4}+\beta_a+\beta_b-2\gamma-2\sqrt{\varepsilon-\beta_b+\gamma}\sqrt{\gamma+\frac{1}{4}}} \tag{20}$$

Also from Eq.(A11),we get λ_n as

$$\lambda_n = n^2+n+2n\left(\sqrt{\varepsilon-\beta_b+\gamma}+\sqrt{\gamma+\frac{1}{4}}\right) \tag{21}$$

By setting equations (20) and (21) equal to each other and replacing equation (12), the energy eigenvalues equation of the VHP is obtained.

$$E_{nl} = \frac{\alpha^2h^2l\left(l+1\right)}{2m} + a - \alpha c - \frac{\alpha^2h^2}{2m}\left(\frac{(n+l+1)+\dfrac{l(l+1)+\dfrac{2m(d-c)}{\alpha h^2}-\dfrac{2mab}{\alpha h^2}}{n+l+1}}{}\right)^2 \tag{22}$$

The wave function with the normalization constant in ground and first excited state are given in Eqs.(23) and (24).

$$\psi_{0l}\left(r_q\right) = \sqrt{\frac{\alpha\,\Gamma_{[2(1+A+B)]}}{\Gamma_{[2A]}\,\Gamma_{[2+2B]}}} \times \left(e^{-\alpha r_q}\right)^A \times \left(1-e^{-\alpha r_q}\right)^{B+\frac{1}{2}} \tag{23}$$

$$\psi_{1l}\left(r_q\right)=\sqrt{\frac{2A(3+2A+2B)\alpha\,\Gamma\,[2(1+A+B)]}{(3+2B)\,\Gamma\,[2+2A]\,\Gamma\,[2+2B]}}\times(e^{-\alpha\,r_q})^{A}\times$$

$$(1-e^{-\alpha\,r_q})^{B+\frac{1}{2}}\times \mathrm{P}_1^{(2A,2B)}\left(1-2e^{-\alpha\,r_q}\right) \quad (24)$$

where

$$A=\sqrt{l\times(l+1)-\frac{2m}{\alpha^2h^2}\times(E_{nl}-a)-\frac{2m\times\alpha c}{\alpha^2h^2}}$$

$$B=l+\frac{1}{2}$$

The momentum space wave function is,

$$\Psi_{00}(p)=\sqrt{\frac{1}{2\pi}}\sqrt{\frac{\alpha\,\Gamma\,[2(1+A+B)]}{\Gamma\,[2A]\,\Gamma\,[2+2B]}}\int_0^{\infty}(e^{-\alpha\,r_q})^{A}\times(1-$$

$$e^{-\alpha\,r_q})^{B+\frac{1}{2}}e^{-ip\,r_q}\,d\,r_q \quad (25)$$

$$\Psi_{00}(p)=\sqrt{\frac{\alpha\,\Gamma\,[2(1+A+B)]}{\Gamma\,[2A]\,\Gamma\,[2+2B]}}\times\frac{\Gamma\,[\frac{3}{2}+B]\,\Gamma\,[A+\frac{ip}{\alpha}]}{\sqrt{2\pi}\alpha\,\Gamma\,[\frac{3}{2}+A+B+\frac{ip}{\alpha}]} \quad (26)$$

The SE eigenfunction in spherical polar coordinates is solved in 3D by

$$\Psi_{nlm}\left(r_q,\theta_{r_q},\phi_{r_q}\right)=\frac{R_{nl}(r)}{r}Y_{lm}\left(\theta_{r_q},\phi_{r_q}\right) \quad (27)$$

The Spherical Harmonics $Y_{lm}(\theta,\phi)$ correspond to the solution of the angular component of the Schrödinger equation and is expressed as

$$Y_{lm}(\theta,\phi)=(-1)^m\sqrt{\frac{2l+1(l-m)!}{4\pi(l+m)!}}P_l^m(Cos\theta)e^{im\phi} \quad (28)$$

where the function $P_l^m(Cos\theta)$ is the associated Legendre function.

The wave function in momentum space is represented by the Fourier transform [53].

$$\Psi_{nlm}(p,\theta_p,\phi_p)=\frac{1}{(2\pi)^{3/2}}\int_{\mathbb{R}^3}\Psi_{nlm}\left(r_q,\theta_{r_q},\phi_{r_q}\right)e^{-i\bar{p}.\bar{r}}\,d\,r_q \quad (29)$$

The notation $d\,r_q=\left(r_q^{\,2}d\,r_q\right)sin\theta d\theta d\phi$ is the volume element. The plane-wave expansion for $e^{-i\bar{p}.\overline{r_q}}$ takes the form as [**54**]

$$e^{-i\bar{p}.\bar{r}}=(2\pi)^{3/2}\sum_{l=0}^{\infty}\sum_{m=-l}^{l}i^{-l}\frac{J_{l+1/2}\left(p\,r_q\right)}{\sqrt{p\,r_q}}\,\mathrm{Y}_{lm}(\theta_p,\phi_p)\mathrm{Y}_{lm}^{*}\left(\theta_{r_q},\phi_{r_q}\right) \quad (30)$$

Where $J_{l+1/2}$is the Bessel function.

Due to axial symmetry, only the m=0 terms remain, reducing the plane-wave expansion to

$$e^{-i\bar{p}.\bar{r}}=(2\pi)^{3/2}\mathrm{Y}_{lm}(\theta_p,\phi_p)\sum_{l=0}^{\infty}i^{-l}\frac{J_{l+1/2}\left(p\,r_q\right)}{\sqrt{p\,r_q}}\,\mathrm{Y}_{l0}^{*}\left(\theta_{r_q},\phi_{r_q}\right) \quad (31)$$

Substituting equations (28) and (31) into equation (30) yields

$$\Psi_{nlm}(p,\theta_p,\phi_p)=i^{-l}\mathrm{Y}_{lm}(\theta_p,\phi_p)\int_0^{\pi}\int_0^{2\pi}\mathrm{Y}_{l0}\left(\theta_{r_q},\phi_{r_q}\right)\mathrm{Y}_{l0}^{*}\left(\theta_{r_q},\phi_{r_q}\right)sin\theta d\theta d\phi$$

$$\times\int_0^{\infty}\frac{R_{nl}\left(r_q\right)}{r_q}\frac{J_{l+1/2}\left(p\,r_q\right)}{\sqrt{p\,r_q}}\,r_q^{\,2}\,d\,r_q \quad (32)$$

For the ground state ($n=0,l=0$) and using the orthonormality condition for the Spherical Harmonics

$$\Psi_{000}(p,\theta_p,\phi_p)=\frac{\mathrm{Y}_{00}(\theta_p,\ \phi_p)}{\sqrt{p}}F_{00}(p) \quad (33)$$

where

$$F_{00}(p)=\int_0^{\infty}\sqrt{r_q}\,R_{00}\left(r_q\right)J_{1/2}\left(p\,r_q\right)d\,r_q \quad (34)$$

The integral in equation (34) can be computed using the MATHEMATICA software by utilizing the position wave function expression. The momentum space wave function is derived accordingly as,

$$\Psi_{000}(p,\theta_p,\phi_p)=(-1)^{1/4}e^{-\frac{i\pi}{4}}\Gamma\left[\frac{3}{2}+B\right]\sqrt{\frac{\alpha\,\Gamma\,[2(1+A+B)]}{\Gamma\,[2A]\,\Gamma\,[2+2B]}}\frac{\left(\frac{i\,\Gamma\left[A-\frac{ip}{\alpha}\right]}{\Gamma\left[\frac{3}{2}+A+B-\frac{ip}{\alpha}\right]}+\frac{i\,\Gamma\,\mathrm{a}\left[A+\frac{ip}{\alpha}\right]}{\Gamma\left[\frac{3}{2}+A+B+\frac{ip}{\alpha}\right]}\right)}{p\sqrt{2\pi}\alpha}\mathrm{Y}_{00}(\theta_p,\ \phi_p) \quad (35)$$

3. Results and Discussion

Utilizing the NU method to find the SE eigenstates with VHP in a closed form. Table 1 shows the one-dimensional ground state Shannon entropy for d = 1 with different values of c. As the potential parameter (c) increases, the position space entropy goes up, while the momentum space decreases with higher values of c. One can note that the total entropies follow the BBM inequality. Observing a similar pattern when adjusting the potential parameter d from 1 to 10, with c held constant at 0.1. The table displays the three-dimensional ground state Shannon entropy in Table 2. In this case, the potential parameter d was set to 1, while c was varied from 0.1 to 1.0. There was an increase in position space and a decrease in momentum space, with a total exceeding 6.4343. Observing a consistent outcome when c is set at 0.1 and d ranges from 1 to 10. The sum of the values also meets the BBM inequality in three dimensions. This implies that when position entropy is known more precisely, that is, decreasing, momentum entropy must increase, meaning the momentum is known less precisely. This trade-off is a fundamental aspect of quantum mechanics, reflecting the dual nature of particles as both particles and waves and the inherent limitations on our ability to precisely measure certain pairs of conjugate properties.

Table 1. One-dimensional Ground State Shannon entropy

$h = 1, m = 1, a = 0, b = 0, d = 1, l = 0, n = 0, \alpha = 0.01$

	$d = 1$				$c = 0.1$		
c	$S(r)$	$S(p)$	$S(T) \geq 2.1447$	d	$S(r)$	$S(p)$	$S(T) \geq 2.1447$
0.1	0.558352186	1.820251835	2.378604022	1	0.558352186	1.820251835	2.378604022
0.2	0.675104361	1.703499994	2.378604354	2	-0.184507904	2.563110947	2.378603043
0.3	0.807312204	1.571292634	2.378604838	3	-0.606008840	2.984611720	2.378602880
0.4	0.959701366	1.418904214	2.37860558	4	-0.901613293	3.280216119	2.378602826
0.5	1.139562940	1.239043861	2.378606801	5	-1.129480282	3.508083082	2.378602801
0.6	1.359029861	1.019579166	2.378609027	6	-1.314938432	3.693541219	2.378602787
0.7	1.640619425	0.737994349	2.378613774	7	-1.471323519	3.849926299	2.378602779
0.8	2.034029065	0.344598000	2.378627065	8	-1.606527444	3.985130218	2.378602774
0.9	2.691999426	-0.313306000	2.378693426	9	-1.725609404	4.104212174	2.378602770
1.0	5.453596870	-3.054975192	2.398621678	10	-1.832007844	4.210610612	2.378602768

Table 2. Three-dimensional Ground State Shannon entropy.

$h = 1, m = 1, a = 0, b = 0, d = 1, l = 0, n = 0, \alpha = 0.01$

	$d = 1$				$c = 0.1$		
c	$S(r)$	$S(p)$	$S(T) \geq 6.4342$	d	$S(r)$	$S(p)$	$S(T) \geq 6.4342$
0.1	2.356488661	4.210105084	6.566593745	1	2.356488661	4.210105084	6.566593745
0.2	2.706744186	3.859849958	6.566594144	2	0.127911327	6.438681244	6.566592571
0.3	3.103366265	3.463228459	6.566594724	3	-1.136590993	7.703183368	6.566592375
0.4	3.560531526	3.006064088	6.566595614	4	-2.023404187	6.058972249	4.035568062
0.5	4.100112582	2.466484498	6.566597081	5	-2.707005078	9.273597358	6.566592279
0.6	4.758506661	1.808093094	6.566599755	6	-3.263379488	9.829971751	6.566592263
0.7	5.603261121	0.963344326	6.566605447	7	-3.732534727	10.29912698	6.566592253
0.8	6.783450506	-0.216829244	6.566621263	8	-4.138146485	10.70473873	6.566592247
0.9	8.75716367	-2.190463224	6.566700446	9	-4.495392354	11.06198460	6.566592243
1.0	16.98279444	-10.39165035	6.591144099	10	-4.814587667	11.38117991	6.56659224

Table 3. Three-dimensional Ground State Fisher Information

$h = 1, m = 1, a = 0, b = 0, d = 1, l = 0, n = 0, \alpha = 0.01$

	$d = 1$				$c = 0.1$		
c	$I(r)$	$I(p)$	$I(r)I(p) \geq 36$	d	$I(r)$	$I(p)$	$I(r)I(p) \geq 36$
0.1	13.1768	3.642751741	47.99981	1	13.1768	3.642751741	47.99981114
0.2	10.4328	4.600867777	47.99993	2	58.2168	0.824488281	47.99906934
0.3	8.0088	5.993417858	48.00008	3	135.2568	0.354872211	47.99887971
0.4	5.9048	8.129030139	48.00030	4	244.2968	0.196477482	47.99882003
0.5	4.1208	11.64834918	48.00052	5	385.3368	0.12456343	47.99887357
0.6	2.6568	18.06717879	48.00088	6	558.3768	0.085961509	47.99891224
0.7	1.5128	31.73029037	48.00158	7	763.4168	0.062873883	47.99897888
0.8	0.6888	69.69146674	48.00348	8	1000.4568	0.047977061	47.99897643
0.9	0.1848	259.8105483	48.01299	9	1269.4968	0.037809514	47.99905749
1.0	0.0008	63888.88889	51.11111	10	1570.5368	0.03056232	47.99924751

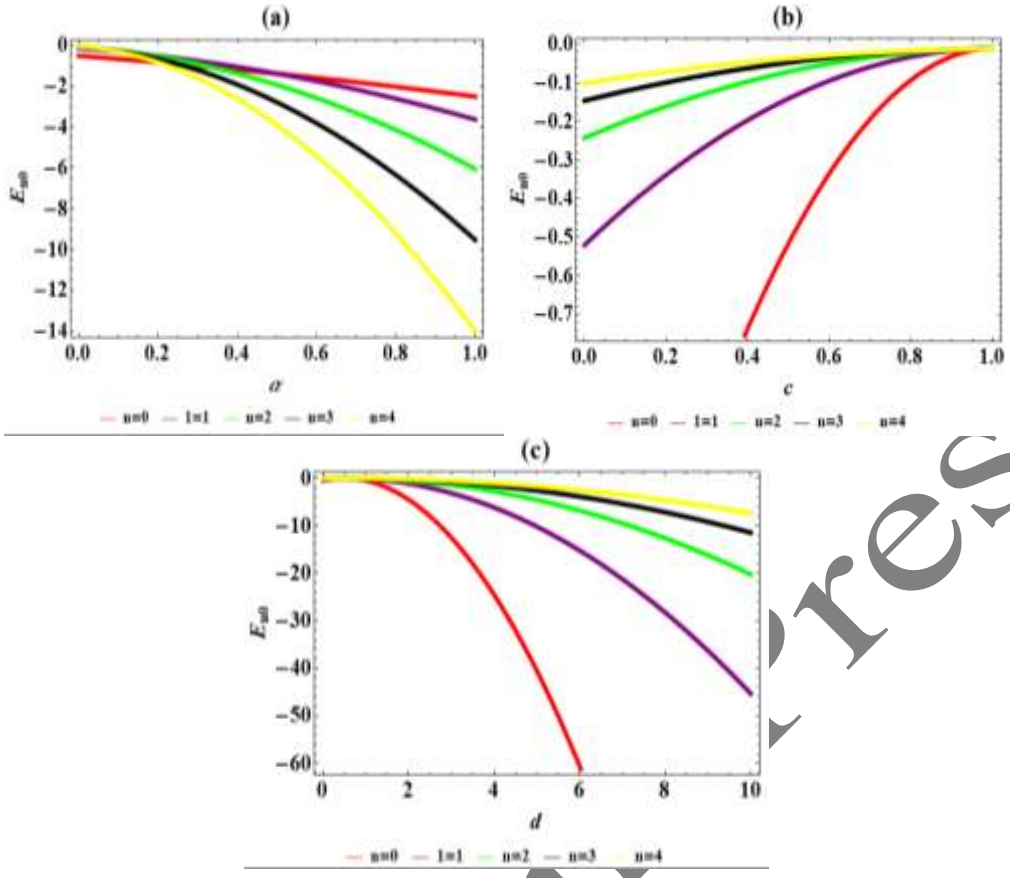

Fig 2. Variation of energy spectra with potential parameters and principal quantum number. $h = 1, m = 1, a = 0, b = 0$

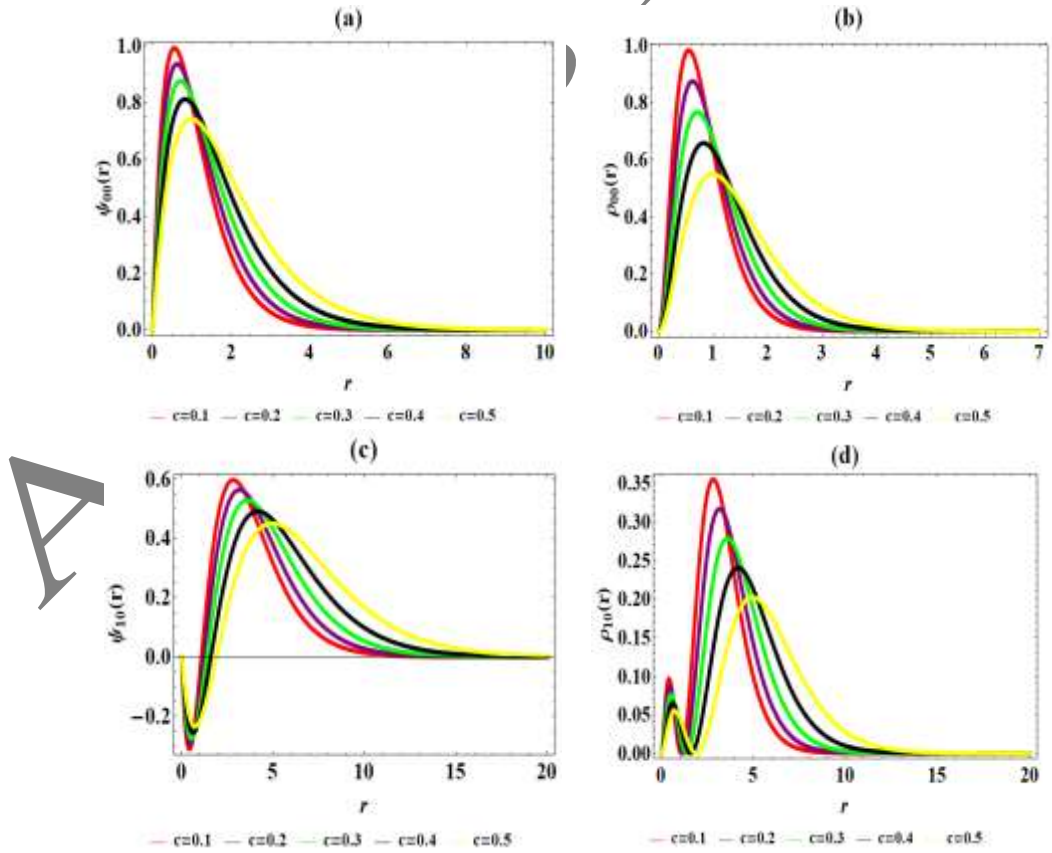

Figure3: Position space ground and first excited state wave function and probability densities. $h = 1, m = 1, a = 0, b = 0, d = 1, l = 0, \alpha = 0.01$

Table 3 presents the three-dimensional ground-state Fisher information. At a constant value of d, the position entropy decreases as the optimizing parameter (c) increases, whereas the momentum space entropy rises as the optimizing parameter (c) for the ground state increases. When the product entropy exceeds 36, the SCR inequality is satisfied. The identical pattern holds true when c remains constant and d is varied between 1 and 10. It is observed that as the position Fisher entropy decreases, indicating a more precise measurement of position, the momentum Fisher entropy must increase. This implies that the Fisher information regarding momentum decreases, resulting in a decrease in the precision of momentum measurement. This demonstrates how position and momentum uncertainties complement each other in quantum mechanics. Looking into the balance between Fisher entropy and momentum reveals a basic part of quantum mechanics' uncertainty principle. It shows how you can't measure certain pairs of related variables with great accuracy at the same time. The variation of energy spectra with respect to potential parameters and the principal quantum number is illustrated in Figure 2(a–c). The energy spectrum is illustrated in Figure 2(a) alongside the screening parameter (SP). As SP increases, it has been observed that energy decreases. The energy spectra are plotted against the PP c in Figure 2b. We observed parabolic curves with distinct minimum turning points that concave upwards prior to a point of convergence. The energy spectrum is represented as a function of the potential parameter d in Figure 2(c). As the value of d increases, the energy decreases exponentially along the vertical axis, resulting in diverging spectral curves. The position space, ground, and first excited state wave function and probability density plot are illustrated in Figure 3(a–d). The wave function plot for the ground state is depicted in Figure 3(a), wherein the maximum point is located at 1. Fig. 3b illustrates the probability density plot pertaining to the ground state. It is quantized according to a Gaussian distribution with distinct peaks. Figure 3(c) illustrates the wave function plot of the first excited state, which reveals a sinusoidal curve featuring local minimum and maximum points. In contrast, Figure 3(d) presents the probability density plot of the first excited state, which deviates from the wave function by displaying distinct peaks that correspond to a particular quantum state and conform to a normal distribution. These graphs are in excellent agreement with other researchers' work in the existing literature.

4. Conclusion

This study used the NU method to study the radial SE for a newly proposed Varshni-Hellmann potential. We used the Greene-Aldrich approximation and a good coordinate transformation procedure to get the energy eigenvalues and normalized wave function through analysis. We investigated the Shannon entropy and FI in position and momentum space using the normalized wave function. Both entropies met the BBM and SCR in one and three dimensions. The ground and fist excited state wave functions and probability density plots were also obtained. Momentum Fisher entropy increases as position Fisher entropy decreases, indicating more precise position measurement. This decreases momentum Fisher information, reducing momentum measurement precision. This shows how quantum mechanics' position and momentum uncertainties work together. The balance between position and momentum Fisher's entropy shows how the uncertainty principle in quantum mechanics limits the precision of measuring certain pairs of conjugate variables simultaneously.

Funding

This research was carried out under LRGS Grant LRGS/1/2020/UM/01/5/2 (9012-00009), Fault-tolerant Photonic Quantum States for Quantum Key Distribution, provided by the Ministry of Higher Education of Malaysia (MOHE).

Acknowledgements

N. Ali, Inyang, E.P. and A.E.L. Aouami, acknowledges the support from the UniMAP Special Research Grant-International Postdoctoral with grant number: 9004-00100.

Conflicts of interest/Competing interests

No conflicting interests are stated by the authors.

Availability of data and material

This article contains all of the materials used and all data generated or analyzed during this investigation.

Authors' contributions

Inyang E. P., A.E.L. Aouami, and Ali N. formulated the problem, wrote the full manuscript, and presented the results and graphics. Endut R. performed computational analysis. Aljunid S.A. and N. R. Ali progresses by creating the literature, carefully reviewing it, and making essential revisions to the manuscript. All authors have reviewed and endorsed the final manuscript.

5. References

1. J Obu, et al., *Jordan J. Phys.* **16, 3** (2023) 329.
2. C O Edet, et al., *Eur. Phys. J. Plus* **138, 10** (2023) 904.
3. E P Inyang, *Indian J. Phys.* (Online), **95, 12** (2021) 2733.
4. E Omugbe, et al., *J. Mol. Model*. **30, 3** (2024) 1.
5. E P Inyang, et al., *East Europ. J. Phys.* **1** (2024) 156.
6. R Khalid, *Phys. Scr.* **99** (2024) 025234.
7. E Omugbe, et al., *Phys. Scr*. **96, 12** (2021) 125408.
8. E P Inyang, et al., *East Europ. J. Phys.* **1** (2023) 53.

9. M Abu-Shady, E Omugbe, and E P Inyang, *J. Niger. Soc. Phys. Sci*. (2024) 1771.
10. A N Ikot, et al., *Eur. Phys. J. Plus* **137, 12** (2022) 1370.
11. E P Inyang, et al., *Eur. Phys. J. Plus* **38, 11** (2023) 969.
12. E P Inyang, et al., *Canad. J. Phys.* **99, 11** (2021) 982.
13. P O Amadi, et al., *Int. J. Quant. Chem.* **120, 14** (2020) e26246.
14. C E Shannon, 1948. *Bell Syst. Tech. J.* **27, 3** (1984) 379.
15. S Kullback and R A Leibler, *Ann. Math. Stat*. **22, 1** (1951) 79.
16. S Kullberg, "*Information theory and statistics*" Wiley, New York (1959).
17. T M Cover and J A Thomas, (1988). *IEEE Trans. Inf. Theory* **29** (1983) 5. *Sci.* **34** 724.
18. R A Fisher, "*Theory of statistical estimation*" Cambridge University Press (1925).
19. S B Sears, R G Parr, and U Dinur, 1980. *Isr. J. Chem*. **19, 1-4** (1980) 165.
20. C Tsallis, *Europ. Phys. J.* A **40, 3** (2009) 257.
21. A Renyi, "*Proc. 4th Symp. on Mathematics, Statistics and Probability*" (1960).
22. O Onicescu, *C. R. Acad. Sci. Ser.* AB **263** (1966) 841.
23. E Omugbe, *Indian J. Phys*. **97, 12** (2023) 3411.
24. S Majumdar, N Mukherjee, and A K Roy, *Chem. Phys. Lett.* **716** (2019) 257.
25. G H Sun and S H Dong, *Phys. Scr*. **87, 4** (2013) 045003.
26. M S Abdelmonem, A Abdel-Hady, and I Nasser, *Mol. Phys*. **115, 13** (2017) 1480.
27. I Białynicki-Birula and J Mycielski, *Commun. Math. Phys*. **44** (1975) 129.
28. R O Esquivel, M Molina-Espíritu, and S López-Rosa, *J. Phys. Chem*. A **127, 30** (2023) 6159.
29. J S Dehesa, et al., *Int. J. Quant. Chem*. **110, 8** (2010) 1529.
30. Y J Shi, et al., *Laser Phys*. **27, 12** (2017) 125201.
31. C A Onate, et al., *Int. J. Quant. Chem*. **119, 19** (2019) e25991.
32. C N Isonguyo, K J Oyewumi, and O S Oyun, *Int. J. Quant. Chem*. **118, 15** (2018) e25620.
33. E Romera and J S Dehesa, *Phys. Rev*. A **50, 1** (1994) 256.
34. M C Onyeaju, et al., *J. Mol. Model*. **29, 10** (2023) 311.
35. H G Laguna, S J Salazar, and R P Sagar, *J. Math. Chem*. **60, 7** (2022) 1422.
36. I J Njoku, et al., *Int. J. Quant. Chem*. **123, 6** (2023) e27050.
37. F Ayedun, et al., *East Europ. J. Phys*. **4** (2022) 87.
38. C R Estañón, et al., *Int. J. Quant. Chem*. **124, 4** (2024) e27358.
39. I J Njoku, et al., *Phys. Open*, **15** (2023) 100152.
40. N Sobrino-Coll, et al., *J. Stat. Mech.: Theory Exp*. **2017, 8** (2017) 083102.
41. A K Roy, *Mod. Phys. Lett*. A **29, 21** (2014) 1450104.
42. E P Inyang, E S William, and J A Obu, *Rev. Mex. Fis*. **67, 2** (2021) 193.
43. H Hellmann, *J. Chem. Phys*. **3, 1** (1935) 61.
44. P Aspoukeh and S M Hamad, *Chin. J. Phys*. **68** (2020) 224.
45. V K Gryaznov, *Zh. Eksp. Teor. Fiz*. **79** (1980) 125.
46. L Kleinman and J C Phillips, *Phys. Rev*. **116, 4** (1959) 880.
47. A J Hughes and J Callaway, *Phys. Rev.* **136, 5A** (1964) A1390.
48. Y P Varshni and R C Shukla, *Rev. Mod. Phys*. **35, 1** (1963) 130.
49. E P Inyang, E P Inyang, and E S William, *Jordan J. Phys.* **14, 4** (2021) 337.
50. T C Lim and R A Udyavara, *C. Europ. J. Phys.* **7** (2009) 193-197.
51. E S William, E P Inyang, and E A Thompson, *Rev. Mex. Fis*. **66, 6** (2020) 730.
52. R L Greene and C Aldrich, *Phys. Rev*. A **14, 6** (1976) 2363.
53. A F Nikiforov and V B Uvarov, "*Special functions of mathematical physics*" Springer (1988).
54. E P Inyang, et al., *Rev. Mex. Fis.* **68** (2022) 1.

Appendix A: Review of Nikiforov-Uvarov (NU) method

The NU method according to Nikiforov and Uvarov is used to transform Schrödinger-like equations into a second-order differential equation through a coordinate transformation $x = x(r)$, of the form [55,56]

$$\psi''(x) + \frac{\tilde{\tau}(x)}{\sigma(x)}\psi'(x) + \frac{\tilde{\sigma}(x)}{\sigma^2(x)}\psi(x) = 0 \tag{A1}$$

where $\tilde{\sigma}(x),$ and $\sigma(x)$ are polynomials, at most second degree and $\tilde{\tau}(x)$ is a first-degree polynomial. The exact solution of Eq. (A1) can be obtained by using the transformation

$$\psi(x) = \phi(x)y(x) \tag{A2}$$

This transformation reduces Eq.(A1) into a hypergeometric-type equation of the form

$$\sigma(x)y''(x)+\tau(x)y'(x)+\lambda y(x)=0 \tag{A3}$$

The function $\phi(x)$ can be defined as the logarithm derivative

$$\frac{\phi'(x)}{\phi(x)}=\frac{\pi(x)}{\sigma(x)} \tag{A4}$$

With $\pi(x)$ being at most a first-degree polynomial. The second part of the wave functions in Eq. (A2) is a hypergeometric-type function obtained by Rodrigues relation:

$$y(x)=\frac{N_{nl}}{\rho(x)}\frac{d^n}{dx^n}\left[\sigma^n(x)\rho(x)\right] \tag{A5}$$

where N_{nl} is the normalization constant and $\rho(x)$ the weight function which satisfies the condition below;

$$\left(\sigma(x)\rho(x)\right)'=\tau(x)\rho(x) \tag{A6}$$

where also

$$\tau(x)=\tilde{\tau}(x)+2\pi(x) \tag{A7}$$

For bound solutions, it is required that

$$\frac{d\tau(x)}{dx}<0 \tag{A8}$$

The eigenfunctions and eigenvalues can be obtained using the definition of the following function $\pi(x)$ and parameter λ, respectively:

$$\pi(x)=\frac{\sigma'(x)-\tilde{\tau}(x)}{2}\pm\sqrt{\left(\frac{\sigma'(x)-\tilde{\tau}(x)}{2}\right)^2-\tilde{\sigma}(x)+k\,\sigma(x)} \tag{A9}$$

and

$$\lambda=k_{-}+\pi_{-}'(x) \tag{A10}$$

The value of k can be obtained by setting the discriminant in the square root in Eq. (17) equal to zero. As such, the new eigenvalues equation can be given as

$$\lambda_n+n\tau'(x)+\frac{n(n-1)}{2}\sigma''(x)=0,(n=0,1,2,...) \tag{A11}$$